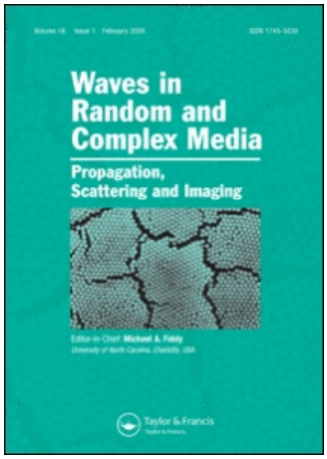

Waves in Random and Complex Media

Publication details, including instructions for authors and subscription information:
http://www.informaworld.com/smpp/title~content=t716100762

Three-dimensional electromagnetic nonlinear inversion in layered media by a hybrid diagonal tensor approximation: Stabilized biconjugate gradient fast Fourier transform method

To cite this Article: , 'Three-dimensional electromagnetic nonlinear inversion in layered media by a hybrid diagonal tensor approximation: Stabilized biconjugate gradient fast Fourier transform method', Waves in Random and Complex Media, 17:2, 129 - 147
To link to this article: DOI: 10.1080/17455030601016117
URL: http://dx.doi.org/10.1080/17455030601016117

Waves in Random and Complex Media
Vol. 17, No. 2, May 2007, 129–147

Three-dimensional electromagnetic nonlinear inversion in layered media by a hybrid diagonal tensor approximation: Stabilized biconjugate gradient fast Fourier transform method

BAOJUN WEI, ERGÜN ŞIMŞEK, CHUN YU and QING HUO LIU*

Department of Electrical & Computer Engineering, Duke University, Durham, NC 27708, USA

(Received 4 April 2006; in final form 13 September 2006)

This paper presents an efficient three-dimensional nonlinear electromagnetic inversion method in a multilayered medium for radar applications where the object size is comparable to the wavelength. In the first step of this two-step inversion algorithm, the diagonal tensor approximation is used in the Born iterative method. The solution of this approximate inversion is used as an initial guess for the second step in which further inversion is carried out using a distorted Born iterative method. Since the aim of the second step is to improve the accuracy of the inversion, a full-wave solver, the stabilized biconjugate-gradient fast Fourier transform algorithm, is used for forward modelling. The conjugate-gradient method is applied at each inversion iteration to minimize the functional cost. The usage of an iterative solver based on the FFT algorithm and the developed recursive matrix method combined with an interpolation technique to evaluate the layered medium Green's functions rapidly, makes this method highly efficient. An inversion problem with 32 768 complex unknowns can be solved with 1% relative error by using a simple personal computer. Several numerical experiments for arbitrarily located source and receiver arrays are presented to show the high efficiency and accuracy of the proposed method.

1. Introduction

Three-dimensional (3-D) electromagnetic inverse scattering has widespread applications in geophysical exploration and biomedical imaging. The development of fast and accurate algorithms is crucial for the solution of inverse scattering problems since usually the characterization of the buried targets needs to be performed *in situ*. However, this may be a complicated and challenging task, especially for buried objects. The challenges arise from the nonlinear, non-unique, and ill-posed properties of the problem, as well as the forward solver. Over the past few decades, several numerical techniques have been proposed to circumvent the inherent difficulties in different inverse scattering applications, see [1–19] for some three-dimensional implementations.

*Corresponding author: E-mail: qhliu@ee.duke.edu

Waves in Random and Complex Media
ISSN: 1745-5030 (print), 1745-5049 (online)
http://www.tandf.co.uk/journals
DOI: 10.1080/17455030601016117

In inverse scattering, the main goal is the determination of the quantitative description of the unknown scatterer(s), such as its size, location, permittivity, and conductivity, from measurement data obtained away from the scatterer. The forward scattering solver is required in most inversion methods [20–32]. For the numerical solution, the volume integral equation is an appropriate choice since the reconstruction domain is an inhomogeneous medium in most applications. It is well known that iterative methods, e.g. the conjugate-gradient (CG) method and biconjugate-gradient (BCG) method, are much more efficient than direct full-wave solvers, such as the Method of Moments (MoM) [21–32]. For this reason, the stabilized biconjugate-gradient/fast Fourier transform algorithm (BCGS-FFT) has been chosen as a full-wave forward solver [25, 27, 28]. However, for some applications, a good approximation of the solution is of interest. In this direction, several approximation techniques have been developed based on either the Born or the Rytov approximations over the past few decades, such as the Born approximation, the extended Born approximation (EBA) [22,23,33–35], the quasi-linear (QL) and quasi-analytical (QA) approximations [10–15], and the diagonal tensor approximation (DTA) [19, 20]. DTA expresses the scattered fields inside objects as the projection of the background fields via a second-rank scattering tensor (a reflectivity tensor) which is approximated as a source-dependent diagonal tensor based on the principle of superposition. Numerical tests show that DTA has high accuracy and wide range of applicability. Note that DTA is an approximate method, so it is in general not as accurate as full-wave solvers, but our results showed that it is satisfactory for contrasts significantly higher than other approximations.

Once the fields for a given model are obtained, the scatterer can be reconstructed via an inversion method such as the contrast source inversion (CSI) method [14, 16, 20, 29], the Born (BIM) and distorted Born (DBIM) iterative methods [30, 38, 39], among others. The CSI method constructs a sequence of contrast sources and contrasts iteratively without using a forward solver. It is a stable method but requires a large number of iterations to obtain desired accuracy. BIM and DBIM are commonly used iterative methods for the solution of nonlinear inverse scattering problem since they usually require fewer iterations. The main difference between BIM and DBIM is that the latter updates the background Green's function for each iteration. Due to this difference, DBIM is computationally more expensive than BIM, but it has the advantage of second-order convergence, whereas BIM has only first-order convergence. This computational cost/convergence order trade-off can be handled in two-step algorithms in different ways. One possibility is the frequency hopping approach that uses lower frequency data as an initial guess to the higher frequency problem [20, 40–43]. Since the Born approximation works well at low frequencies, one can obtain better images and faster convergence after several steps of frequency hopping than using the high-frequency data directly. Another possibility is that one can obtain a rough distribution of the unknown contrast quickly by using an approximate method, such as DTA, within BIM. This quickly obtained approximate solution can be used as an initial guess for DBIM and hence the solution can be obtained by using fewer iterations than regular DBIM implementation.

In this manner, we develop an efficient inverse scattering algorithm based on the BIM/DTA and DBIM/BCGS-FFT algorithms to reconstruct both the permittivity and conductivity of 3-D dielectric objects buried in a lossy multilayered medium for the radar applications. In this algorithm, inversion is a two-step process:

Step-1: Obtain the contrast distribution roughly via BIM, by using the approximate fields obtained with DTA at each step of BIM.

Step-2: Use the contrast distribution obtained in the first step as an initial guess for DBIM with BCGS-FFT as the forward solver for field data and Fréchet derivatives.

In other words, in this two-step algorithm, we first obtain a rough approximation of the inversion, then we improve its accuracy. Numerical results show that this is an efficient and accurate method when the object size is comparable to the wavelength, even for the problems with multiple scatterers and limited measurement data.

Different than the previous works of our research group [19, 30, 31] in which DBIM and contrast-source inversion (CSI) method have been implemented, here we develop a hybrid BIM/DTA and DBIM/BCGS-FFT algorithm. The developed recursive dyadic Green's function method makes it possible to solve the problems with source/receiver arrays located in any layer, whereas in [19, 30, 31], they have both been limited in the first layer of the multi-layered medium, even though in principle any locations are possible.

The structure of the paper is as follows: In section 2, the integral equations and the forward modelling method, DTA, are briefly introduced first. Then, the procedure followed for the implementation of inversion methods, BIM and DBIM, is described. The numerical results are presented in section 3 and the conclusions are given in section 4.

2. Theory

Consider a general multilayer medium consisting of $N + 1$ layers separated by N planar interfaces parallel to the xy plane, as shown in figure 1. Layer i exists between z_{i-1} and z_i and is characterized by relative permittivity $\epsilon_{r,i}$ and conductivity σ_i. Assume that the sources and receivers may be in multiple layers, for example, in layer p and m, a reconstruction domain, D, is chosen in layer q, which includes all the unknown objects to be detected. The electrical properties of layer q, layer m and the objects are characterized by the complex

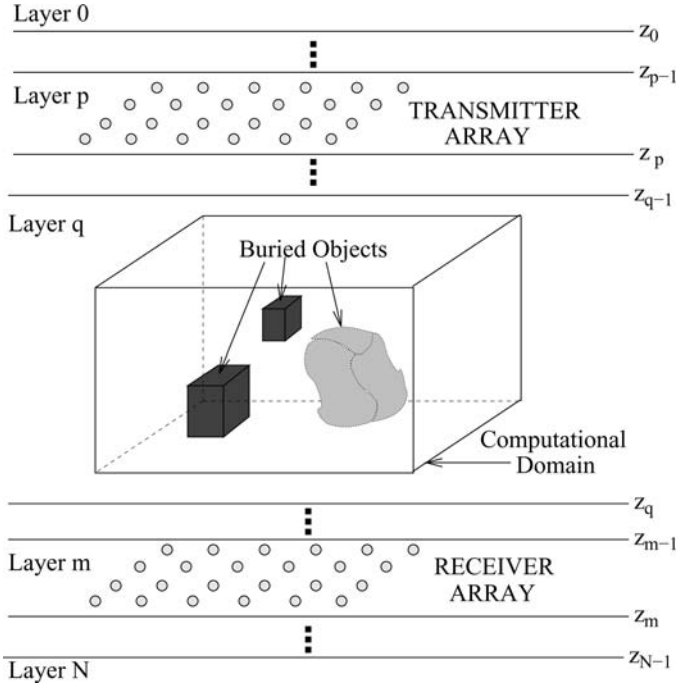

Figure 1. General scattering problem with 3D objects buried in a multilayer medium. The sources and receivers are located in layers p and m, respectively. A reconstruction domain is chosen in layer q to enclose all the unknown objects to be imaged. The electrical properties of layer q, layer m and the objects are characterized by complex permittivities $\tilde{\epsilon}_q$, $\tilde{\epsilon}_m$ and $\tilde{\epsilon}$, respectively.

permittivities $\tilde{\epsilon}_q$, $\tilde{\epsilon}_m$ and $\tilde{\epsilon}$, respectively, which are the combinations of the corresponding material's relative dielectric constant and conductivity. For example, the complex permittivity for an inhomogeneous object is expressed as $\tilde{\epsilon} = \epsilon_0\epsilon_r - j\sigma/\omega$, where ϵ_r is the relative dielectric constant of the object, ϵ_0 the permittivity of free space, σ the conductivity of the object, j the imaginary unit, and ω the angular frequency. In this paper, we assume that the magnetic permeability μ in the target is the same as μ_q in the layered medium. The transmitter and receiver arrays are arbitrarily located electric or magnetic dipoles.

2.1 *Integral equations and forward modelling*

The total electric field at $\mathbf{r}$, inside the dielectric object, created by an exciting source located at $\mathbf{r}_T$ can be written as a summation of the incident and scattered fields based on the superposition principle as follows

$$\mathbf{E}(\mathbf{r}, \mathbf{r}_T) = \mathbf{E}^{\text{inc}}(\mathbf{r}, \mathbf{r}_T) + \left(k_q^2 + \nabla\nabla\cdot\right)\int_D \mathbf{G}_{qq}^{AJ}(\mathbf{r}, \mathbf{r}')\cdot\chi(\mathbf{r}')\mathbf{E}(\mathbf{r}', \mathbf{r}_T)d\mathbf{r}', \quad \mathbf{r}\in D \tag{1}$$

where $\mathbf{G}_{qq}^{AJ}(\mathbf{r}, \mathbf{r}')$ is an auxiliary dyadic Green's function representing the magnetic vector potential, the wavenumber in layer q is given by $k_q^2 = \omega^2\mu_q\tilde{\epsilon}_q$ and $\chi(\mathbf{r})$ is the contrast defined as

$$\chi(\mathbf{r}) = \frac{\tilde{\epsilon}(\mathbf{r})}{\tilde{\epsilon}_q} - 1. \tag{2}$$

Equation 1 is called the object equation, which is a Fredholm integral equation of the second kind for the unknown field inside the object. In fact, equation 1 can also be written by using the electric dyadic Green's function, $\mathbf{G}_{mq}^{EJ}$. However, $\mathbf{G}_{qq}^{AJ}$ has weaker singularity than $\mathbf{G}_{mq}^{EJ}$ [36]. Hence, in the forward modelling, we use $\mathbf{G}_{qq}^{AJ}$ to solve equation 1 for the total electric field inside D. Once the total electric field is obtained, the scattered field at any location on S can be calculated as

$$\mathbf{E}_m^{sca}(\mathbf{r}, \mathbf{r}_T) = j\omega\tilde{\epsilon}_q\int_D \mathbf{G}_{mq}^{EJ}(\mathbf{r}, \mathbf{r}')\cdot\chi(\mathbf{r}')\mathbf{E}(\mathbf{r}', \mathbf{r}_T)d\mathbf{r}', \quad \mathbf{r}\in S \tag{3}$$

where $\mathbf{G}_{mq}^{EJ}(\mathbf{r}, \mathbf{r}')$ is the electric dyadic Green's function at the observation point $\mathbf{r}$ in layer m related to a unit current source at the point $\mathbf{r}'$ in layer q. Equation 3 is called the data equation which defines the scattered field at the observation point.

The solutions of these integral equations can be obtained numerically by using full-wave solvers such as MoM and BCGS-FFT, or they can be approximated by using approximation methods such as EBA and DTA. Approximate methods do not provide results as accurate as full-wave solvers, but they can produce good approximations of the exact solution by using much less CPU time and memory than full-wave solvers, which can be used as a good initial guess for an iterative solver. In this work, we use DTA because of its high accuracy and wide range of applicability to approximate the fields inside the objects. Briefly, the basic idea of the DTA is to approximate the scattered field internal to the scatterer by a source-dependent diagonal scattering tensor $\Gamma(\mathbf{r}, \mathbf{r}_T) = \text{diag}[\gamma_x, \gamma_y, \gamma_z]$ so that the scattered field for $\mathbf{r}\in D$ can be written as

$$\mathbf{E}^{sca}(\mathbf{r}, \mathbf{r}_T) \approx \Gamma(\mathbf{r}, \mathbf{r}_T)\cdot\mathbf{E}^{\text{inc}}(\mathbf{r}, \mathbf{r}_T) \qquad \mathbf{r}\in D. \tag{4}$$

The details of this method can be found in [19, 31, 32]. As mentioned before, in this work we use DTA as a fast-forward solver/approximate method during each iteration of BIM to produce an initial distribution of the contrast. In the second step of the inversion, we use BCGS-FFT algorithm as a full-wave solver to form a hybrid DBIM/BCGS-FFT algorithm to

improve the accuracy of the inversion. The details of the BCGS-FFT algorithm can be found in [25, 27, 28].

2.2 *The inverse scattering method*

Assume that there are M_T illuminating sources to excite the medium and M_R receivers to collect the scattered field. As a result, the total number of data points collected is $M = M_T \times M_R$. Suppose the reconstruction domain D is discretized into N small cells and the field quantities are linear and the contrast function is constant in each cell. The integral equation 3, which relates the measured data and the unknown contrast of the material, can be discretized as follows,

$$\mathbf{f}(\mathbf{r}_{i_R}, \mathbf{r}_{i_T}) = \omega\tilde{\epsilon}_q \sum_{k=1}^{N} \mathbf{G}_{mq}^{EJ}(\mathbf{r}_{i_R}, \mathbf{r}'_k) \cdot \mathbf{E}(\mathbf{r}'_k, \mathbf{r}_{i_T})\chi(\mathbf{r}'_k)\Delta V \tag{5}$$

with the trapezoidal rule, where $\mathbf{f}$ is a $3M$-dimensional data column vector whose elements are the given measured scattered electric field data, ΔV is the volume element, $i_R = 1, \cdots, M_R$ and $i_T = 1, \cdots, M_T$ denote indices for the receiver and transmitter, respectively. For M measurements and N discretized cells, 5 can be written compactly as

$$\mathbf{f} = \mathbf{A}\mathbf{x}, \tag{6}$$

where $\mathbf{x}$ is an N-dimensional column vector of the contrast function χ, and $\mathbf{A}$ is a $3M \times N$ matrix whose elements are given by

$$\mathbf{A}_{ik} = j\omega\tilde{\epsilon}_q \mathbf{G}_{mq}^{EJ}(\mathbf{r}_{i_R}, \mathbf{r}'_k) \cdot \mathbf{E}(\mathbf{r}'_k, \mathbf{r}_{i_T})\Delta V \tag{7}$$

where $i = i_R + (i_T - 1)M_R$, and $k = 1, \cdots, N$.

Since the total field $\mathbf{E}$ within the objects is an unknown function of the material contrast function χ, 6 is a nonlinear equation. Moreover, the limited amount of information makes the problem non-unique. This equation can be solved iteratively by using either the BIM [37] or DBIM [38, 39]. In this work, we implement a two-step inversion as follows.

Step-1:DTA-BIM

Since the BIM has been shown to be an efficient and stable algorithm in the inverse scattering problem, and DTA is an efficient and satisfactory approximation method, we can obtain a rough distribution of the unknown contrast quickly by combining these two methods. In DTA, equation 7 is approximated by

$$\mathbf{A}_{ik} \approx j\omega\tilde{\epsilon}_q \mathbf{G}_{mq}^{EJ}(\mathbf{r}_{i_R}, \mathbf{r}'_k) \cdot [\mathbf{I} + \Gamma(\mathbf{r}'_k, \mathbf{r}_{i_T})] \cdot \mathbf{E}^{\text{inc}}(\mathbf{r}'_k, \mathbf{r}_{i_T})\Delta V \tag{8}$$

where the components of Γ are updated for the each iteration. The contrast function at the $(n+1)$th iteration, χ_{n+1}, is obtained by minimizing the following normalized cost function

$$F_{n+1}(\mathbf{x}) = \frac{||\mathbf{f} - \mathbf{M_n}\mathbf{x_{n+1}}||_{\mathbf{S}}^2}{||\mathbf{f}||_{\mathbf{S}}^2} + \gamma^2 \frac{||\mathbf{x_{n+1}}||_{\mathbf{D}}^2}{||\mathbf{x_n}||_{\mathbf{D}}^2}, \tag{9}$$

where γ is the regularization parameter, $||\cdot||_{S(D)}^2$ denotes the L_2 norm on the S or D domain. This linear least squares problem is equivalent to the following expression which can be solved by the conjugate gradient (CG) method

$$\left(\frac{\mathbf{M}_n^\dagger \mathbf{M}_n}{||\mathbf{f}||_{\mathbf{S}}^2} + \frac{\gamma^2}{||\mathbf{x_n}||_{\mathbf{D}}^2}\mathbf{I}\right)\mathbf{x}_{n+1} = \frac{\mathbf{M}_n^\dagger \mathbf{f}}{||\mathbf{f}||_{\mathbf{S}}^2}, \tag{10}$$

where the superscript † denotes the complex conjugate transposition. The ill-posed behaviour of the problem requires a nonzero regularization parameter. However, to be able to keep the

first term of the right hand side of 9 as the dominant term, γ should be much smaller than 1. For these reasons, γ is chosen as a constant number between 0.01 and 0.05 in this work. Numerical results show that the solution does not change significantly when different γ values are used within this interval.

Note that the electric dyadic Green's function $\mathbf{G}_{mq}^{EJ}$ is evaluated for the layered background without considering the existence of χ. This is done only once and stored for repeated use in each iteration of BIM.

Step-2: BCGS-DBIM

The DBIM has a different procedure than BIM. The DBIM starts with the contrast distribution obtained from the first step and calculates the fields. Then the contrast function is updated for this new field distribution and this process is repeated until an acceptable solution is achieved or until a predefined number of iterations is completed. However, unlike BIM, the DBIM requires updating $\mathbf{G}_{mq}^{EJ}$ for the each iteration. For a given contrast distribution χ, we can calculate the fields by evaluating the integral in 1 with BCGS-FFT which uses the regular layered media Green's functions. However, to update the contrast distribution for the given fields, we need to obtain matrix $\mathbf{A}$ considering the distribution of $\mathbf{x_n}$ in the layered background. So, we cannot simply use the layered media Green's functions. In this case, $\mathbf{G}_{mq}^{EJ}$ can be obtained by using the reciprocity theorem from the total electric field which is calculated using BCGS-FFT by replacing the source and field points.

In DBIM, the normalized cost function at the $(n+1)$th iteration is defined as

$$F_{n+1}(\delta\mathbf{x}) = \frac{||\delta\mathbf{f} - \mathbf{M_n}\delta\mathbf{x_{n+1}}||_{\mathbf{S}}^2}{||\mathbf{f}||_{\mathbf{S}}^2} + \gamma^2 \frac{||\delta\mathbf{x_{n+1}}||_{\mathbf{D}}^2}{||\mathbf{x_n}||_{\mathbf{D}}^2}, \tag{11}$$

which is equivalent to the following expression

$$\left(\frac{\mathbf{M}_n^\dagger \mathbf{M}_n}{||\mathbf{f}||_{\mathbf{S}}^2} + \frac{\gamma^2}{||\mathbf{x_n}||_{\mathbf{D}}^2}\mathbf{I}\right)\delta\mathbf{x}_{n+1} = \frac{\mathbf{M}_n^\dagger \delta\mathbf{f}}{||\mathbf{f}||_{\mathbf{S}}^2}, \tag{12}$$

where $\delta\mathbf{f}$ denotes the error between the measured scattered field and the predicted scattered field, and $\delta\mathbf{x}_{n+1}$ is the correction of $\mathbf{x_n}$ during the $(n+1)$th iteration.

The evaluation of the electric dyadic Green's functions in layered background is a time-consuming and memory-occupying step of the whole procedure. To speed up this process and to reduce the memory requirement, we develop a recursive matrix method combined with an interpolation technique. In this recursive matrix method, the components of the electric dyadic Green's function $\mathbf{G}^{EJ}(\mathbf{r}, \mathbf{r}')$ are formulated as the combinations of six Sommerfeld integrals, which only depend on ρ, z, and z'; where $\rho = \sqrt{(x-x')^2 + (y-y')^2}$. So we only need to calculate and store these six Sommerfeld integrals with respect to each z and z' pair for some ρ values in advance, and then we can calculate the Green's functions at the desired points with interpolating the pre-calculated components. This technique reduces the CPU time and computer memory usage dramatically and makes it possible to solve a complicated problem with arbitrarily located source/receiver arrays.

3. Numerical results

To demonstrate the efficiency of this two-step algorithm, we show the inversion results at the end of each step. The solution of step-1 is the solution obtained by using BIM in which DTA is used for the forward modelling at each iteration. The solution of step-2 is the solution obtained using DBIM in which BIM solution is chosen as an initial guess and BCGS-FFT is

used for the forward modelling at each iteration. For all the examples, the dimensions of the voxels are chosen in such a way that the sampling density is always larger than 10 points per wavelength (PPW) and the same voxel size is used to perform both simulation and inversion.

3.1 *Four cuboids in a five-layer background*

In this example, we have a five-layer background with four cuboids buried in the third layer, see figure 1 for the general schema. The electric parameters of the background are: $\epsilon_{r0} = 1.0$, $\sigma_0 = 0.0$ S/m; $\epsilon_{r1} = 3.0, \sigma_1 = 0.01$ S/m; $\epsilon_{r2} = 2.0, \sigma_2 = 0.01$ S/m; $\epsilon_{r3} = 3.0, \sigma_3 = 0.01$ S/m; $\epsilon_{r4} = 1.0$, $\sigma_4 = 0.0$ S/m. The interface positions are at $z_0 = 0.0$ m, $z_1 = 0.02$ m, $z_2 = 0.156$ m and $z_3 = 0.176$ m. The imaging domain D in the middle layer is centred at (0.0, 0.0, 0.088) m and has the dimensions of $0.106 \times 0.106 \times 0.106$ m^3. The operating frequency of the vertical electric dipoles is $f = 2$ GHz. Inside the reconstruction domain D, there are four cuboids with the electric parameters $\epsilon_r = 4.0$ and $\sigma = 0.2$ S/m. The objects centred at (0.0, -0.028, 0.088) m and (0.0, 0.028, 0.088) m have the dimensions of $0.021 \times 0.017 \times 0.03$ m^3. The objects centred at (-0.028, 0.0, 0.088) m and (0.028, 0.0, 0.088) m have the dimensions of $0.017 \times 0.021 \times 0.03$ m^3.

The 2-D planar source array is in the top layer with a distance of 0.02 m above z_0. It has 8×8 sources which are uniformly distributed within the range from -0.28 m to 0.28 m both in x and y directions. The receiver array is in the bottom layer with a distance of 0.02 m below z_3 and has the same configuration with the source array. In this case, only z component of the measured scattered fields is used, so the total number of information is $M = 4096$. In all the examples, the synthetic measured scattered fields are generated by the BCGS-FFT method. The imaging domain D is divided into $25 \times 25 \times 25$ voxels, which results in 17 PPW sampling density. The total number of the complex unknowns to be reconstructed is $N = 15\,625$.

Figure 2 compares the relative error of the two-step DTA/DBIM algorithm with the one obtained by using the DBIM algorithm only (background field and contrast are used as the initial guess for the solution) as a function of iteration number; figures 3 and 4 show the reconstructed dielectric constant and conductivity on the xy plane and xz plane at the end of the first and second steps of the inversion, respectively. The effect and importance of the

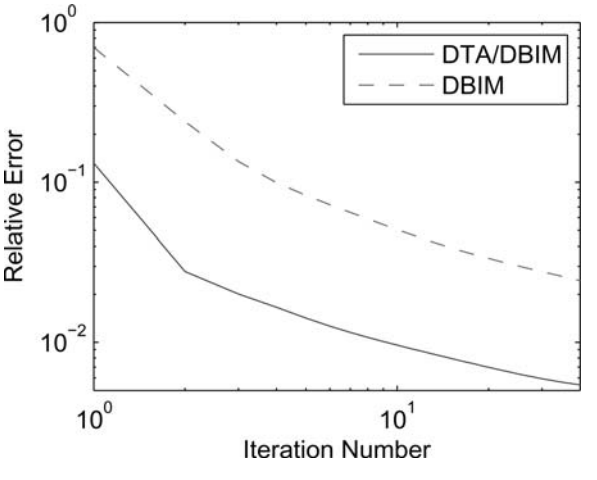

Figure 2. Comparison of the relative error for the hybrid method (two-step DTA-BIM/BCGS-DBIM method abbreviated as DTA/DBIM in the figure) and the regular DBIM algorithm as a function of iteration number for the example described in Section 3.1.

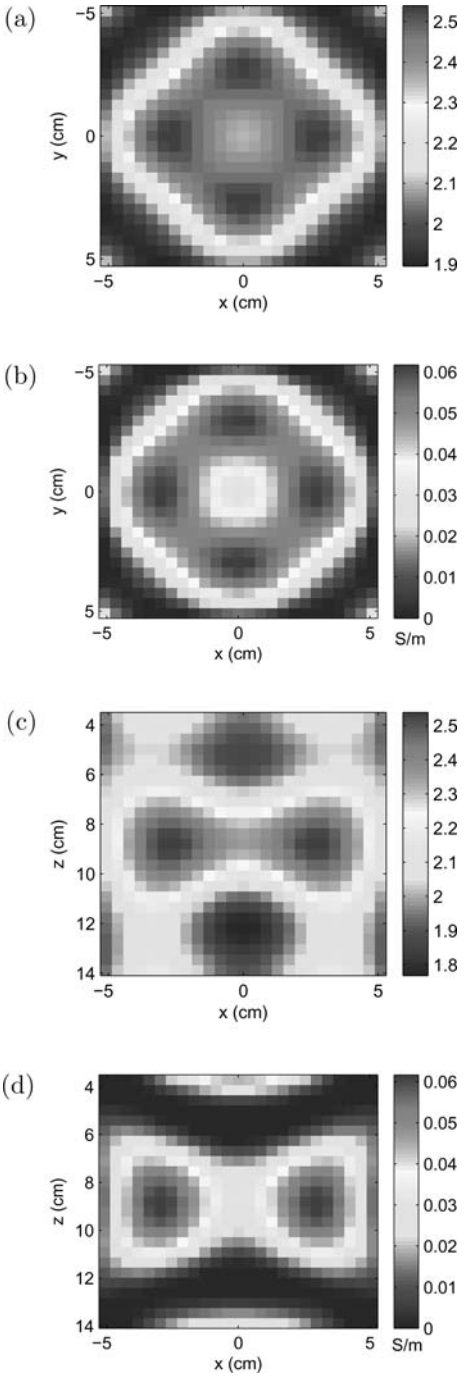

Figure 3. Reconstructed images at the end of the first step of the two-step algorithm for a five-layer background model with four cuboids with the electric parameters $\epsilon_r = 4.0$ and $\sigma = 0.2$ S/m buried in the middle layer where $\epsilon_{r,2} = 2.0$ and $\sigma_2 = 0.01$ S/m. (a) and (b) depict reconstructed dielectric constant and conductivity, respectively, on the xy plane at $z = 8.8$ cm. (c) and (d) depict the reconstructed dielectric constant and conductivity, respectively, on the xz plane at $y = 0.0$.

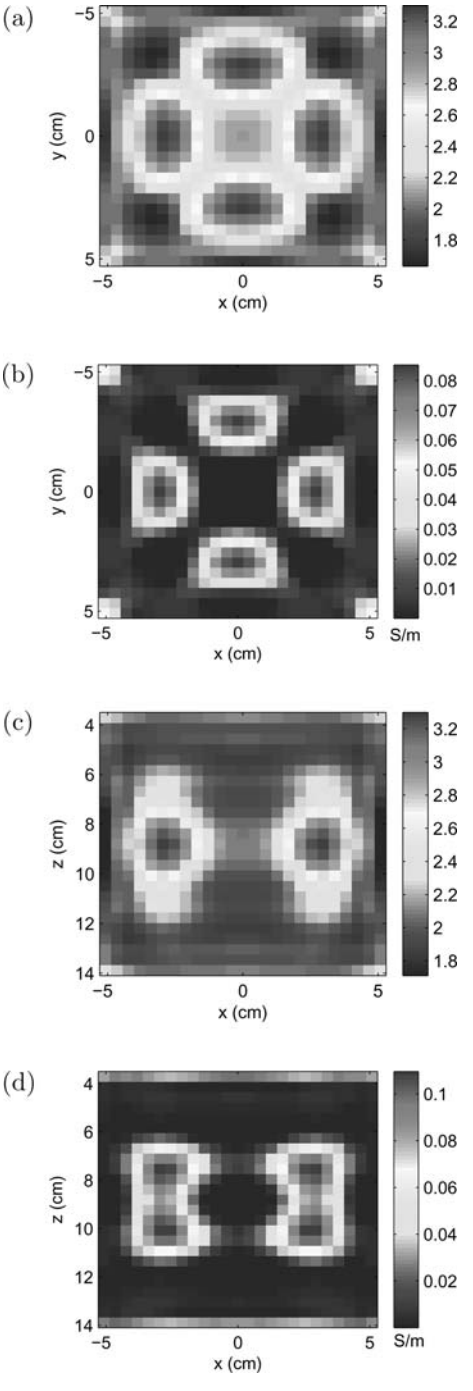

Figure 4. Same as figure 3, except that they are obtained at the end of the second step of the two-step algorithm.

first step of the proposed DTA/DBIM method is clearly depicted in figure 2. By the help of a good initial guess, we can obtain 1% accuracy by using 10 iterations only with the proposed method, however when we use DBIM only, we need more than 40 iterations to obtain the same accuracy. When we compare figures 3 and 4, we can see that the imaging results of DBIM are much more precise than BIM, as expected. Figure 4 shows that the locations and the sizes of the four cuboids are accurately reconstructed, even though the information is much more limited compared with the number of unknowns. We can also see from figure 4 that the resolutions in the x and y directions are higher than that in z direction because the information is collected only on the xy plane. This case successfully demonstrates the capability of our proposed imaging technique in the reconstruction of 3-D objects buried in layered media.

3.2 *Application in microwave biomedical imaging*

The following example is an application of our proposed imaging technique in microwave biomedical imaging to detect breast tumours, which was studied previously for homogeneous background media in [17, 18], among others. In [17] we use the combination of the extended Born approximation (EBA) and CSI method in 2D. In [18] the CSI method is used for 3D imaging assuming the background is homogeneous. Thus, in these previous studies, we did not consider the chest wall effects. In this work we include such effects by simplifying the background as a layered medium. Note that even though the chest wall is not flat and has a finite extent, the layered medium background assumption provides a more realistic model than a homogeneous medium assumption.

For the dielectric properties of the breast tissue utilized in this model, the reader is referred to [17] and the references therein. Here, we have a three-layer background with four cuboids in the top layer. The electric parameters of the background are: $\epsilon_{r0} = 16.0$, $\sigma_0 = 0.16$ S/m; $\epsilon_{r1} = 20.0$, $\sigma_1 = 0.2$ S/m; $\epsilon_{r2} = 1.0$, $\sigma_2 = 0.0$ S/m. The interface positions are at $z_0 = 0.01$ m, $z_1 = 0.2$ m. The imaging domain D in the top layer is centred at (0.0, 0.0, −0.08) m and has the dimensions of $0.16 \times 0.16 \times 0.16$ m^3. The operating frequency of the vertical electric dipoles is $f = 800$ MHz. In D domain, there are four cuboids located at (0.04, 0.04, −0.08), (0.04, −0.04, −0.08), (−0.04, 0.04, −0.08), and (−0.04, −0.04, −0.08) m. For the first and forth cuboids, $\epsilon_r = 32$ and $\sigma = 0.8$ S/m. For the other two, $\epsilon_r = 48$ and $\sigma = 0.4$ S/m.

The sources and receivers are evenly distributed over five surfaces of D, leaving the bottom surface open. There are nine sources or receivers on each surface, so the total number of collected data points is $M = 45 \times 45 = 2025$. The imaging domain D is divided into $32 \times 32 \times 32$ voxels, which results in 13 PPW sampling density. The total number of the complex unknowns to be reconstructed is $N = 32\,768$.

Since the top layer's relative permittivity is quite large with respect to free space, the usage of dielectric contrast, χ_d, might be useful for the comparison where χ_d can be defined as follows

$$\chi_d = \frac{\epsilon_r}{\epsilon_{r,b}} - 1. \tag{13}$$

First let us focus on the case when the dimensions of the objects are $2 \times 2 \times 2$ cm^3. Figure 5 shows the cross-sections of the 3-D reconstructed results at the end of each step. We observe that the locations of the four cuboids are accurately reconstructed and the imaging patterns for the dielectric contrast and conductivity are very close to the model. Clearly, the second step of the inversion improves the accuracy. For this case, the maximum dielectric contrast has reached to 0.69 and the maximum conductivity has reached to 0.37 S/m after 40 iterations using BCGS-DBIM, and the relative data error has been decreased to 0.5%. Although the ratio

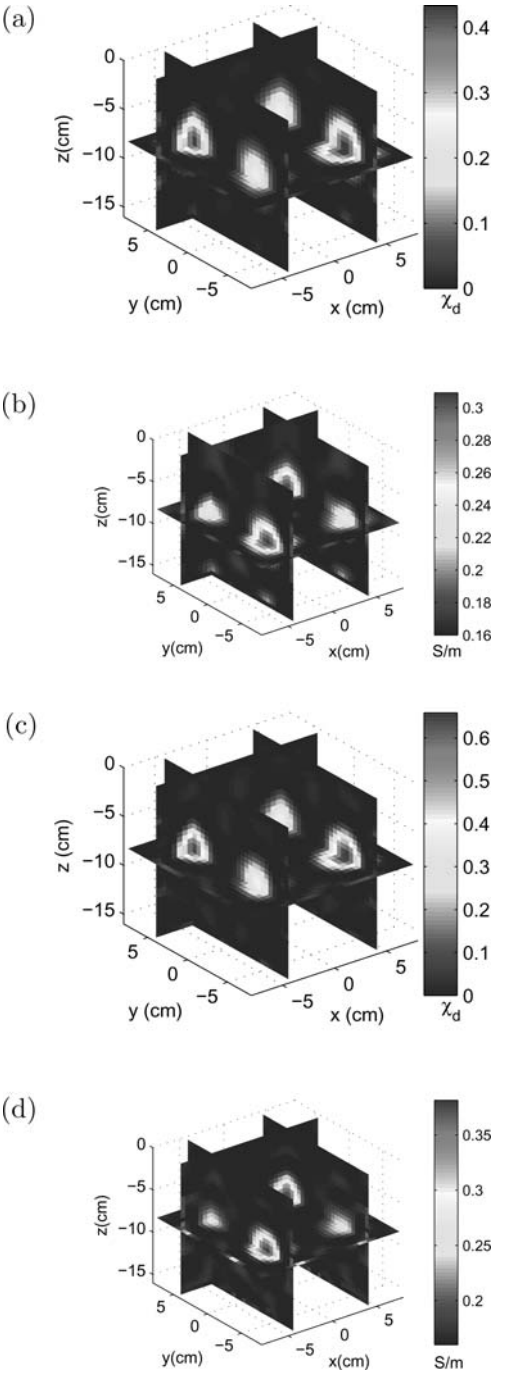

Figure 5. Reconstructed images for a three-layer background model with four cuboids in the top layer when the dimensions of the objects are $2 \times 2 \times 2$ cm^3. The first and fourth cuboids have the same electrical properties: $\chi_{d,c1} = \chi_{d,c4} = 1, \sigma_{c1} = \sigma_{c4} = 0.8$ S/m. The second and third cuboids have the same electrical properties: $\chi_{d,c2} = \chi_{d,c3} = 2$, $\sigma_{c2} = \sigma_{c3} = 0.4$ S/m. The conductivity of the image domain is 0.16 S/m. (a) and (b) depict the reconstructed dielectric contrast function and conductivity, respectively, at the end of first step of the presented algorithm. More accurate images are obtained at the end of the second step shown as (c) and (d) for χ_d and σ, respectively.

M/N in this case is much smaller than the previous example, the resolution of this example is much better due to the volumetric distribution of the sources and receivers.

Figures 6 and 7 show the cross-sections of the 3-D reconstructed results at the end of each step when the dimensions of the objects are $1 \times 1 \times 1$ cm^3 and $0.5 \times 0.5 \times 0.5$ cm^3, respectively. For both cases, the imaging results keep the same patterns as the model, however the reconstructed electrical parameter gets closer to the background parameters as we decrease the scattered fields by decreasing the size of the objects. For the former case, the maximum dielectric contrast has reached 0.82 and the maximum conductivity has reached 0.187 S/m after 40 iterations. For the latter case, the maximum dielectric contrast has reached 0.01 and the maximum conductivity has reached 0.163 S/m after 40 iterations.

In the following case, the dimensions of the first and second objects are $2 \times 2 \times 2$ cm^3, while the dimensions of the third and fourth objects are $1 \times 1 \times 1$ cm^3. Figure 8 gives the cross-sections of the 3-D reconstructed results at the end of each step. The reconstructed dielectric contrast and conductivity of the third and fourth objects are much smaller than the value of the first and second objects. For this case, the imaging patterns for the dielectric contrast and conductivity of the two big objects are very close to the model. The maximum dielectric constant has reached 0.63 and the maximum conductivity has reached 0.36 S/m after 40 iterations.

In the last case, the first example of this section is repeated. However, to appraise the influence of the wrong background information, the background is assumed to be homogeneous ($\epsilon_{r,b} = 16$ and $\sigma_b = 0.16$ S/m) during the inversion. As can be seen from figure 9 the reconstructed images are as successful as the ones shown in figure 5 because of the lower contrast between layers 1 and 2, and the loss in the second layer. This example clearly indicates that this hybrid method of capable of obtaining satisfactory inversion results even without having a 100% accurate background information. However, as the layer contrasts increase and loss decreases, one expects that the mismatch effects will become more significant, see [44] for more examples.

Figure 10 shows the convergence of the relative error in the second step of the inversion as a function of iteration number for the different cases presented in this example. By using a good initial guess provided by the first step, 1% accuracy can be obtained using 40 or less iterations.

All of these results demonstrate that the spatial properties of the buried objects can be reconstructed. However, the accuracy of the reconstructed dielectric constant and conductivity dramatically depends on the size of the objects.

4. Discussions

Both simulation and inversion programs were compiled with the Fortran 77 UNIX compiler on a Dell Optiplex GX260 desktop with Intel P4 2.4 GHz processor and 1024M RAM. The same voxel sizes are used in the forward and inversion. However, it should be noted that two different methods are employed to synthesize (BCGS-FFT) and to invert data (first by the DTA/BIM); the DTA is significantly different from the full-wave BCGST-FFT method, even though the subsequent inversion is refined by the DBIM/BCGS method. Since, this algorithm is specifically developed for radar applications where the object size is comparable to the wavelength, and, at least 10 PPW sampling density is used for the image domain discretization to obtain accurate results, this hybrid algorithm is capable of imaging objects bigger than $0.1\lambda \times 0.1\lambda \times 0.1\lambda$. The usage of higher sampling density makes it possible to reconstruct smaller objects. However, the higher is the sampling density, the higher is the CPU time and memory requirement. Due to the efficiency of the iterative solver (BCGS) and very low CPU time and memory requirements ($O(N \log N)$ and $O(N)$, respectively, where N is the

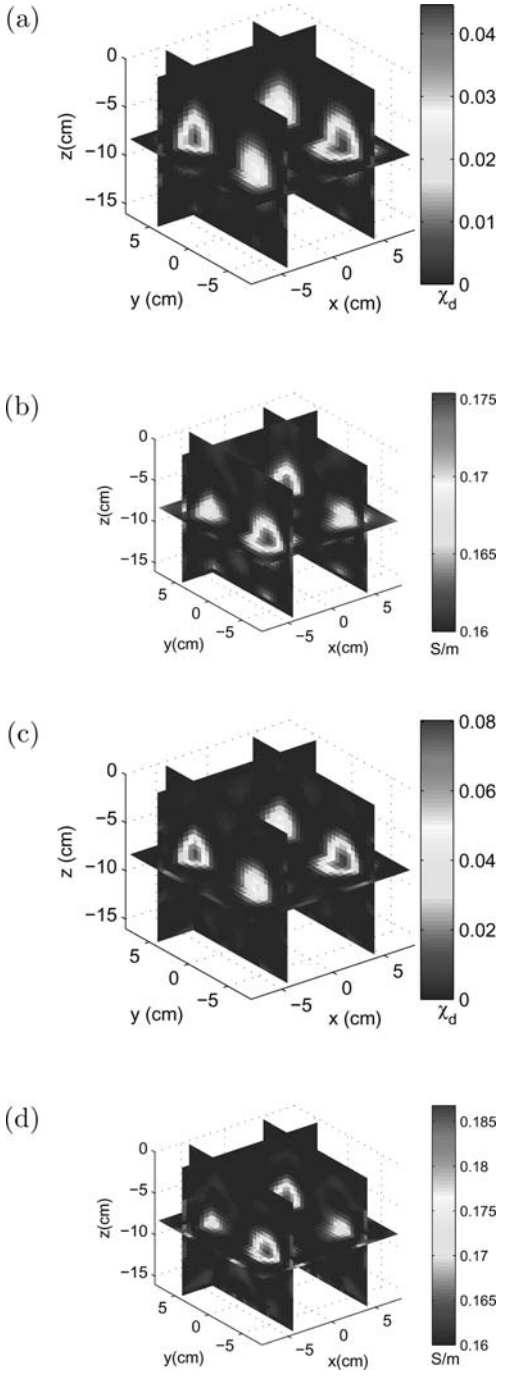

Figure 6. Same as figure 5 except the dimensions of the objects are $1 \times 1 \times 1$ cm^3. The reconstructed dielectric function (a) and conductivity (b) after the first step, and after the second step (c) and (d).

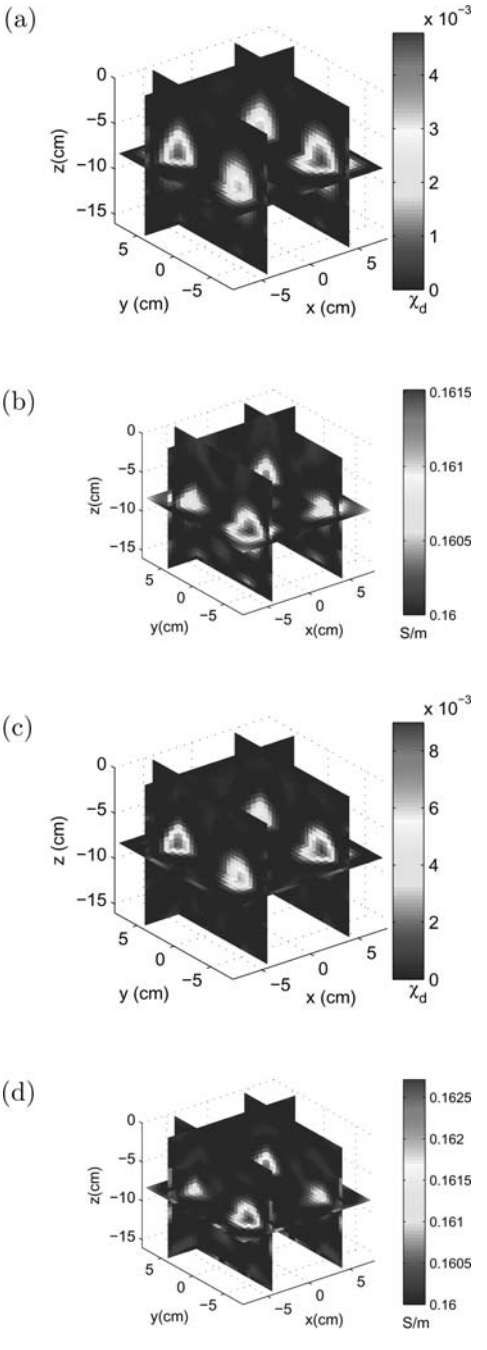

Figure 7. Same as figure 5 except the dimensions of the objects are $0.5 \times 0.5 \times 0.5$ cm^3. The reconstructed dielectric function (a) and conductivity (b) after the first step, and after the second step (c) and (d).

number of the unknowns) of the FFT algorithm, we could solve problems with 32 768 complex unknowns by using a simple PC. Moreover, due to high accuracy of the hybrid method and the size of the object(s) with respect to wavelength, we have not experienced any inversion yielding negative values of dielectric permittivity or electrical conductivity.

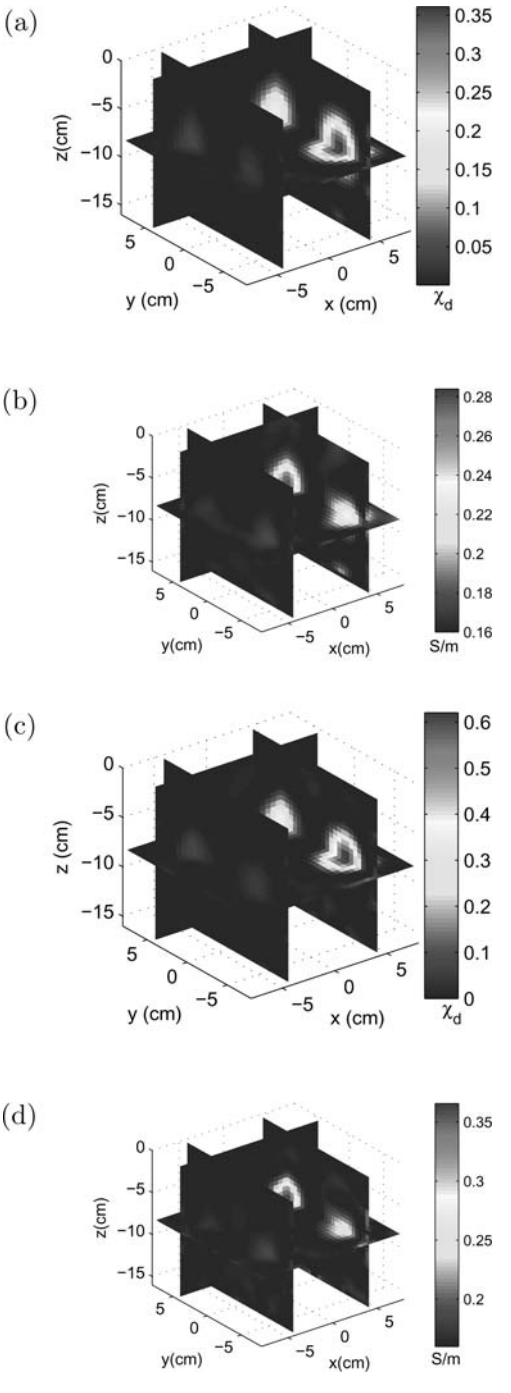

Figure 8. Reconstructed images for a three-layer background model with four cuboids in the top layer when the dimensions of the first two objects are $2 \times 2 \times 2$ cm^3 and the dimensions of the other two objects are $1 \times 1 \times 1$ cm^3. $\chi_{d,c1} = \chi_{d,c4} = 1$, $\sigma_{c1} = \sigma_{c4} = 0.8$ S/m. $\chi_{d,c2} = \chi_{d,c3} = 2$, $\sigma_{c2} = \sigma_{c3} = 0.4$ S/m. The conductivity of the image domain is 0.16 S/m. (a) and (c) depicts the reconstructed contrast function at the end of first and second steps of the two-step algorithm, respectively. (b) and (d) are reconstructed conductivity images at the end of first and second steps, respectively.

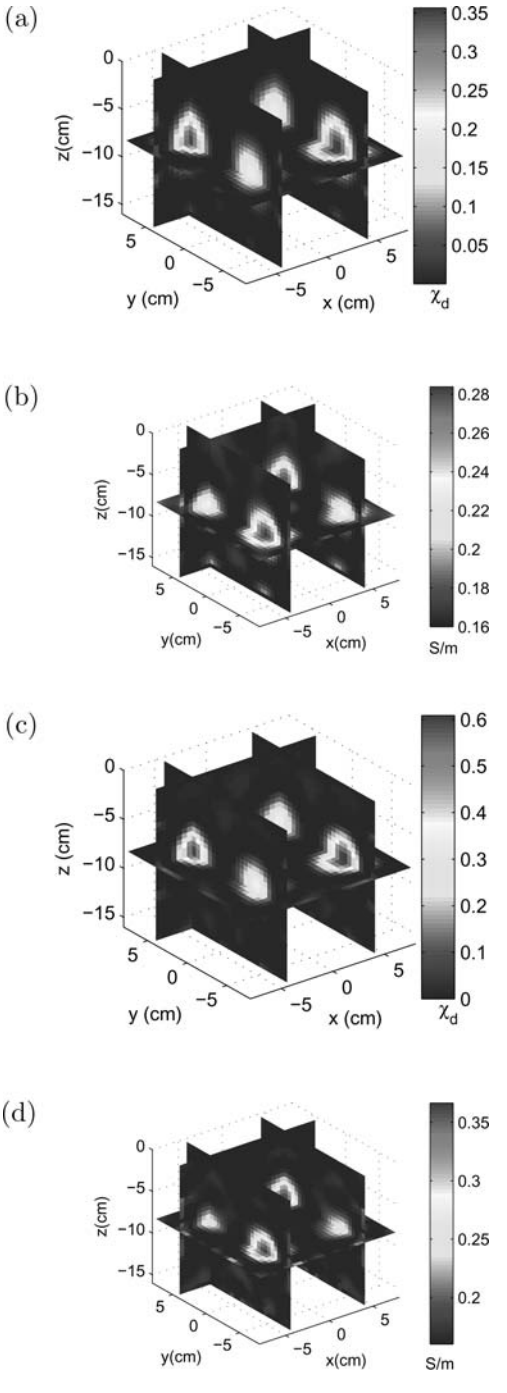

Figure 9. Reconstructed images for a three-layer background model with four cuboids in the top layer when the dimensions of the objects are $2 \times 2 \times 2$ cm^3. To appraise the influence of a wrong background information, the background is assumed to be homogeneous ($\epsilon_{r,b} = 16$ and $\sigma_b = 0.16$ S/m) during the inversion. $\chi_{d,c1} = \chi_{d,c4} = 1$, $\sigma_{c1} = \sigma_{c4} = 0.8$ S/m. $\chi_{d,c2} = \chi_{d,c3} = 2, \sigma_{c2} = \sigma_{c3} = 0.4$ S/m. (a) and (b) depicts the reconstructed dielectric contrast function ($\chi_d = [(\epsilon_r/\epsilon_{r,b}) - 1]$) and the conductivity ($\sigma$), respectively, at the end of first step of the hybrid method. (c) and (d) are the reconstructed contrast function and conductivity images, respectively, at the end of the second step of the inversion.

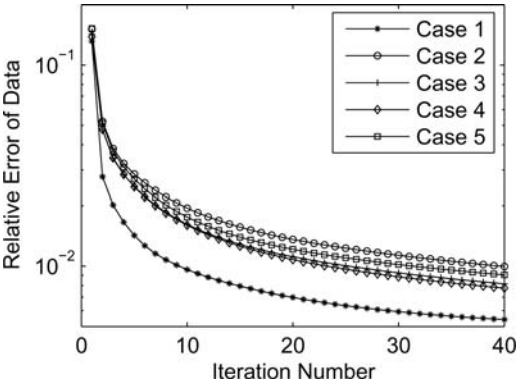

Figure 10. Relative data error of the second step (BCGS-DBIM) of the presented algorithm as a function of iteration number for five different cases presented in Section 3.2.

It should be noted that this hybrid method is constructed on the volume integral equation and FFT algorithm, the volume integral equation solver is not an appropriate choice to solve the problems with little volume current, when the conductivity is very high. As a result, the surface integral equation solvers may be more appropriate for the problems with very conductive objects. For all the presented numerical examples, the conductivity of the object is chosen relatively small because of this reason.

5. Conclusion

An efficient two-step electromagnetic nonlinear inversion method based on the hybridization of the diagonal tensor approximation (DTA) and stabilized biconjugate-gradient fast Fourier transform (BCGS-FFT) method has been developed for the radar and biomedical imaging applications to reconstruct 3-D objects in a multilayered medium. This two-step, hybrid method is referred to as the DTA/BCGS method. In the first step, we combine DTA with the Born iterative method (BIM) to obtain an approximation of the contrast rapidly. Numerical results show that at the end of the first step, 10% relative error can be obtained. This inversion is then used in the second step as the initial solution and is further refined by the distorted Born iterative method (DBIM) with the BCGS-FFT method as the forward solver. The relative error can be decreased to 1% using 40 iterations or less. The efficiency and accuracy of the proposed method has been supported with several numerical experiments, including a microwave biomedical imaging example, for arbitrarily located source and receiver arrays.

References

[1] Eaton, P. A., 1989, 3D EM inversion using integral equations. *Geophysical Prospecting*, **37**, 407–426.
[2] Madden, T. R. and Mackie, R. L., 1989, 3D magnetotelluric modeling and inversion. *Proceedings of the IEEE*, **77**, 318–332.
[3] Smith, J. T. and Booker, J. R., 1991, Rapid inversion of 2 and 3D magnetotelluric data. *Journal of Geophysical Research*, **96**, 3905–3922.
[4] Xiong, Z., 1992, EM modeling of 3D structures by the method of system iteration using integral equations. *Geophysics*, **57**, 1556–1561.
[5] Oristaglio, M., Wang, T., Hohmann, G. W. and Tripp, A., 1993, Resistivity imaging of transient EM data by conjugate-gradient method. *Society of Exploration Geophysicsts Abstracts*, (Washington DC: SEG), 347–350.
[6] Pellerin, L., Johnston, J. and Hohmann, G. W., 1993, 3D inversion of EM data. *Society of Exploration Geophysicsts Abstracts* (Washington, DC: SEG), 360–363.

[7] Lee, K. H. and Xie, G., 1993, A new approach to imaging with low frequency EM fields. *Geophysics*, **58**, 780–796.
[8] Torres-Verdin, C. and Habashy, T. M., 1994, Rapid 2.5-dimensional forward modeling and inversion via a new nonlinear scattering approximation. *Radio Science*, **29**, no. 4, 1051–1079.
[9] Xie, G. and Lee, K. H., 1995, Nonlinear inversion of 3D EM data. *PIERS Proceedings, The University of Washington*, p 323.
[10] Zhdanov, M. S. and Fang, S., 1996, Three-dimensional quasi-linear electromagnetic inversion. *Radio Science*, **31**, 741–754.
[11] Zhdanov, M. S. and Fang, S., 1996, Quasi-linear approximation in 3-D electromagnetic modeling. *Geophysics*, **61**, 646–665.
[12] Zhdanov, M. S. and Fang, S., 1997, Quasi-linear series in three-dimensional electromagnetic modeling *Radio Science* **32**, 2167–2188.
[13] Alumbaugh, D. L. and Newman, G. A., 1997, Three-dimensional massively parallel inversion II. Analysis of a cross-well electromagnetic experiment. *Geophysical Journal International*, **128**, 355–363.
[14] Abubakar, A. and van den Berg, P. M., 1998. Three-dimensional nonlinear inversion in cross-well electrode logging. *Radio Science*, **33**, 989–1004.
[15] Zhdanov, M. S., Dmitriev, V. I., Fang, S. and Hursan, G., 2000, Quasi-analytical approximations and series in electromagnetic modeling. *Geophysics*, **65** 1746–1757.
[16] Abubakar, A., van den Berg, P. M. and Semenov, S. Y., 2002, Two- and three-dimensional algorithms for microwave imaging and inverse scattering. *Progress In Electromagnetics Research*, **37**, 57–79.
[17] Liu, Q. H., Zhang, Z. Q., Wang, T., Ybarra, G., Nolte, L. W., Bryan, J. A. and Joines, W. T., 2002, Active microwave imaging I: 2-D forward and inverse scattering methods. *IEEE Transactions on Microwave Theory and Techniques*, **50**, 123–133.
[18] Zhang, Z. Q. and Liu, Q. H., 2004, 3D nonlinear image reconstruction for biomedical microwave imaging. *IEEE Transactions on Biomedical Engineering*, **51**, 544–5548.
[19] Song, L. P. and Liu, Q. H., 2004, Fast three-dimensional electromagnetic nonlinear inversion in layered media with a novel scattering approximation. *Inverse Problems*, **20**, S171–S194.
[20] Yu, C., Song, L. P. and Liu, Q. H., 2005, Inversion of multi-frequency experimental data for imaging complex objects by a DTA-CSI method. *Inverse Problems*, **21**, S165–S178.
[21] Zhang, Z. Q. and Liu, Q. H., 2001, Three-dimensional weak-form conjugate and biconjugate-gradient FFT methods for volume integral equations. *Microwave and Optical Technology Letters*, **29**, 350–356.
[22] Zhang, Z. Q. and Liu, Q. H., 2001, The hybrid extended Born approximation and CG-FFHT method for axisymmetric media. *IEEE Transactions on Geoscience and Remote Sensing*, **39**, 710–717.
[23] Liu, Q. H., Zhang, Z. Q. and Xu, X. M., 2001, The hybrid extended Born approximation and CG-FFT method for electromagnetic induction problems. *IEEE IEEE Transactions on Geoscience and Remote Sensing*, **39**, 347–355.
[24] Xu, X. M., Liu, Q. H., and Zhang, Z. Q., 2002, The stabilized biconjugate gradient fast Fourier transform method for electromagnetic scattering. *Journal of the Applied Computational Electromagnetics Society*, **17-1**, no. 1, 97–103.
[25] Xu, X. M. and Liu, Q. H., 2002, The BCGS-FFT method for electromagnetic scattering from inhomogeneous objects in a layered medium. *IEEE Transactions on Antennas and Wireless Propagation Letters*, **1**, 77–80.
[26] Zhang, Z. Q., Liu, Q. H. and Xu, X. M., 2003, RCS computation of large inhomogeneous objects using a fast integral equation solver. *IEEE Transactions on Antennas and Propagation*, **51**, 613–618.
[27] Millard, X. and Liu, Q. H., 2003, A fast volume integral equation solver for electromagnetic scattering from large inhomogeneous objects in layered media. *IEEE Transactions on Antennas and Propagation*, **51**, 2393–2401.
[28] Millard, X. and Liu, Q. H., 2004, Simulation of near-surface detection of objects in layered media by the BCGS-FFT method. *IEEE Transactions on Antennas and Propagation*, **42**, 327–334.
[29] Song, L. P., and Liu, Q. H., 2004, GPR landmine imaging: 2D seismic migration and 3D inverse scattering in layered media. *Radio Science*, **40**, RS1S90.
[30] Li, F., Liu, Q. H. and Song, L. P., 2004, Three-dimensional reconstruction of objects buried in layered media using Born and distorted Born iterative methods. *IEEE Geoscience and Remote Sensing Letters*, **1**, 107–111.
[31] Song, L. P. and Liu, Q. H., 2005, A new approximation to three dimensional electromagnetic scattering. *IEEE Geoscience and Remote Sensing Letters*, **2**, 238–242.
[32] Wei, B., Simsek, E. and Liu, Q. H., Improved diagonal tensor approximation and its hybridization with BCGS-FFT algorithm for accurate simulation of 3-D inhomogeneous objects in layered media. *Waves in Random and Complex Media*, submitted.
[33] Habashy, T. M., Groom, R. W. and Spies, B. R., 1993, Beyond the Born and Rytov approximations: a nonlinear approach to electromagnetic scattering. *Journal of Geophysical Research*, **98(B2)**, 1759–1775.
[34] Torres-Verdin, C. and Habashy, T. M., 1995, A two-step linear inversion of two-dimensional conductivity. *IEEE Transactions on Antennas and Propagation*, **43**, 405–415.
[35] Torres-Verdin, C. and Habashy, T. M., 2001, Rapid numerical simulation of axisymmetric single-well induction data using the extended Born approximation. *Radio Science*, **36**, 1287–1306.
[36] Zwamborn, P. and van den Berg, P. M., 1992, The three dimensional weak form of the conjugate gradient FFT method for solving scattering problems. *IEEE Transactions on Microwave Theory and Techniques*, **9**, 1757–1766.

[37] Wang, Y. M. and Chew, W. C., 1989, An iterative solution of the two-dimensional electromagnetic inverse scattering problem. *International Journal of Imaging Systems and Technology*, **1**, 100–108

[38] Cui, T. J. and Chew, W. C., 2000, Novel diffraction tomographic algorithm for imaging two-dimensional dielectric objects buried under a lossy earth. *IEEE Transactions on Geoscience and Remote Sensing*, **38**, 2033–2041.

[39] Cui, T. J., Chew, W. C., Aydiner, A. A., Chen, S. Y., 2001, Inverse scattering of 2D dielectric objects buried in a lossy earth using the distorted Born iterative method. *IEEE Transactions on Geoscience and Remote Sensing*, **39**, 339–346.

[40] Chew, W. C. and Lin, J.H., 1995, A frequency-hopping approach for microwave imaging of large inhomogeneous bodies. *IEEE Microwave and Guided Wave Letters*, **5**, 439–441.

[41] Haddadin, O. S. and Ebbini, E. S., 1998, Imaging strongly scattering media using a multiple frequency distorted Born iterative method. *IEEE Transactions on Ultrasonics, Ferroelectrics and Frequency Control*, **45**, 1485–1496.

[42] Ma, J., Chew, W.C., Lu, C.C., Song, J., 2000, Image reconstruction from TE scattering data using equation of strong permittivity fluctuation. *IEEE Transactions on Antennas and Propagation*, **48**, 860–867.

[43] Rekanos, I.T. and Tsiboukis, T.D., 2000, A finite element-based technique for microwave imaging of two-dimensional objects. *IEEE Transactions on Instrumentation and Measurement*, **49**, 234–239.

[44] Song, L. P., Liu, Q. H., Li, F., and Zhang, Z. Q., 2005, Reconstruction of three-dimensional objects in layered media: Theory and numerical experiments, *IEEE Transactions on Antennas and Propagation*, **53**, 1556–1561.